
Article:
Ortiz-de-Zarate, G, Madariaga, A, Childs, THC et al. (1 more author) (2022) Surface topography irregularities generated by broaching. CIRP Annals, 71 (1). pp. 105-108. ISSN 0007-8506

https://doi.org/10.1016/j.cirp.2022.03.028

CIRP Annals - Manufacturing Technology

Surface topography irregularities generated by broaching

--Manuscript Draft--

Manuscript Number:	
Article Type:	STC C
Keywords:	Topography; Machining; Broaching
Corresponding Author:	Gorka Ortiz-de-Zarate Mondragon Unibertsitatea Mondragon, Pais Vasco SPAIN
First Author:	Gorka Ortiz-de-Zarate, PhD
Order of Authors:	Gorka Ortiz-de-Zarate, PhD
	Aitor Madariaga, PhD
	Thomas H.C. Childs, PhD
	Pedro J Arrazola, PhD
Abstract:	Surface topography irregularities generated by broaching are analysed. Experimental tests were carried out on three workpiece materials: AISI 1045, Ti-6Al-4V, and Inconel 718, varying the cutting speed, rise per tooth, and rake angle. The experimental results combined with numerical simulation demonstrate that surface topography irregularities result from mechanical rather than thermal effects. Higher surface topography variations are obtained when the force magnitude increases, and when its direction is more perpendicular to the machined surface. Additionally, the Young's modulus of both the workpiece and tool materials plays a fundamental role in topography quality, reducing irregularities when the Young’s modulus is increased.

Contents lists available at SciVerse ScienceDirect

CIRP Annals Manufacturing Technology

Journal homepage: www.elsevier.com/locate/cirp

Surface topography irregularities generated by broaching

Gorka Ortiz-de-Zarate[a], Aitor Madariaga[a] (3), Thomas H.C. Childs[b] (1), Pedro J. Arrazola[a] (1)

[a] *Mondragon Unibertsitatea, Faculty of Engineering, Loramendi 4, Arrasate-Mondragón, 20500, Spain*
[b] *School of Mechanical Engineering, University of Leeds, Leeds LS29JT, UK*

Surface topography irregularities generated by broaching are analysed. Experimental tests were carried out on three workpiece materials: AISI 1045, Ti-6Al-4V, and Inconel 718, varying the cutting speed, rise per tooth, and rake angle. The experimental results combined with numerical simulation demonstrate that surface topography irregularities result from mechanical rather than thermal effects. Higher surface topography variations are obtained when the force magnitude increases, and when its direction is more perpendicular to the machined surface. Additionally, the Young's modulus of both the workpiece and tool materials plays a fundamental role in topography quality, reducing irregularities when the Young's modulus is increased.

Topography, Machining, Broaching

1. Introduction

Although the broaching process has some limitations (e.g., high initial investment and costly consumables), it is still among the most effective machining processes for demanding sectors such as the automotive and aeronautical industries [1]. In fact, broaching is widely used to manufacture critical features of transmission components that must withstand high in-service loads. In the automotive sector, broaching plays an essential role in the manufacturing route of crankshafts, which are commonly made of carbon steels (e.g. AISI 1045) [2]. In aeroengines, broaching is used to manufacture the dovetails and fir-trees that attach the blades of compressor and turbine discs, respectively. Titanium-based alloys (e.g. Ti-6Al-4V), are usually employed in compressors, due to their high strength to weight ratio at intermediate temperatures [3–5]. In the aeroengine hot section, nickel-based alloys (e.g. Inconel 718) are employed in turbine manufacturing [3].

Broaching enables the manufacturing of components with geometric complexity, while delivering high dimensional accuracy (ISO ranging from IT6/IT9), good surface finish (R_a = 0.4–1.6 µm) [6], and high levels of repeatability with short machining times [7]. However, the process has certain peculiarities that are not found in other machining operations. The elevated width of cut coupled with multi-tooth simultaneous cutting produces extremely high loads [1]. In particular, the entry and exit of the teeth, can generate surface topography irregularities as observed by Axinte when broaching Inconel 718 [8]. Axinte found that the periodicity of these irregularities coincided with tool pitch, and suggested that these were the consequence of dynamic effects linked to the stiffness of the machine tool-workpiece system.

Such severe topographical irregularities can lead to non-compliance with established tight geometrical tolerances. Furthermore, they can adversely affect the fretting fatigue behavior in assemblies, such as in fir-tree blade to disc joints [9]. Understanding the phenomena involved in the generation of these topographic irregularities is therefore of great industrial interest, to ensure both the quality and safe working life of the component. To date however, the problem has received scant attention in the research literature. Thus, the main objective of the present paper is to study the phenomena involved in the appearance of surface topography irregularities. To this end, the influence of the workpiece material (AISI 1045, Ti-6Al-4V and Inconel 718), cutting conditions (cutting speed), and tool geometry (rise per tooth and rake angle) are analysed experimentally. An empirical approach is combined with Finite Element Method (FEM) simulation to further understand the experimental results.

2. Methodology

Experimental tests representative of industrial applications were selected. Rectangular slots 15 mm wide were broached using an EKIN RAS 10x160x320 broaching machine. The workpiece materials were AISI 1045, Ti-6Al-4V and Inconel 718. Eight cutting conditions were applied to each, varying the rake angle (γ = 10-20°), rise per tooth (h = 0.01-0.05 mm), and cutting speed (v_c = 2.5-7.5 m/min). All tests were carried out using CUT MAX 600 Houghton oil and a skew angle of 5°. More than three repetitions were performed for each condition to estimate uncertainties.

Four different 15 mm width rectangular broaching tools of T15 High-Speed Steel (HSS) were used, varying the rake angle and rise per tooth as described above. Three broaching tools of each geometry were manufactured to ensure a new set for each material. The relief angle (2.5°), pitch (8 mm), and cutting-edge radius (6±2 µm) were maintained fixed in all tests.

The workpieces were rectangular blocks of ≈ 18 mm thickness and 24 mm depth, which ensured that 2-3 teeth were in contact at the same time, as is the case in industry. All the tests were carried out using the same workpiece clamping system bolted on a Kistler 9225B dynamometer, which in turn was bolted to the machine work table. The clamping setup is illustrated in Fig. 1a. The workpiece overhangs the clamp by 5 mm and the clamping screw line is set back from the surface by 7 mm.

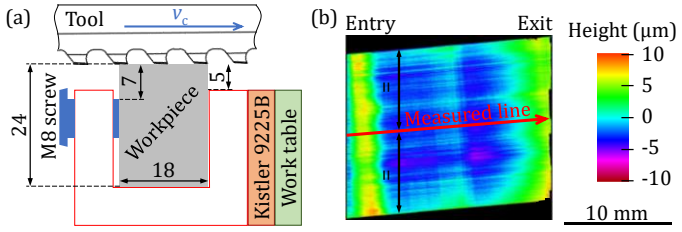

Figure 1. (a) Workpiece clamping system (units in mm), and (b) example surface topography (Inconel 718, v_c = 7.5 m/min, h = 0.05 mm, and γ = 10°).

Broaching forces were measured using a Kistler 9225B dynamometer with a sampling frequency of 20 kHz. Crosstalk was corrected and a low-pass filter with a cut-off frequency of 1 Hz was applied. Finally, the skew angle was corrected to calculate the cutting (F_c) and feed forces (F_f).

The surface topography of all the ≈ 15x18 mm broached slot surfaces was measured using an Alicona IFG4 optical profilometer, an example of which is depicted in Fig. 1b. The 20x magnification objective was used to obtain the 1,107 images that composed each of the surfaces under analysis. The vertical and lateral resolutions were 60 nm and 4 μm, respectively, which means that the surfaces were composed of more than 100 million points. The topography profile was extracted in the middle of the broached slot along the whole broached length (see Fig. 1b), defining a line of 23 profile width (≈ 40 μm). Finally, the data was smoothed by applying the Savitzky-Golay method, using 675 points per window and a 2nd order polynomial.

3. Results

The measured cutting and feed forces F_c and F_f per mm width of cutting edge are presented in Fig. 2 (when three teeth are cutting the actual forces are 45 times the N/mm values in the figure). The ratios F_f/F_c are also included. The larger the F_f/F_c, the steeper the resultant force directed into the workpiece. Forces increase sharply with h, although not five-fold. There are small reductions with increasing γ and v_c. Of most significance for the present work is that the highest forces are obtained for Inconel 718, while the forces for Ti-6Al-4V and AISI 1045 are lower but similar. F_f/F_c decrease with increasing h and γ, and are markedly different between the materials. For Inconel 718, F_f/F_c lies between ≈ 1 and 0.6, for Ti-6Al-4V between 0.84 and 0.36, and for AISI 1045 between 0.45 and 0.25.

Fig. 3 depicts the measured surface profiles. The profile height variations for AISI 1045 (Fig. 3a) are less than those of Ti-6Al-4V (Fig. 3b), and for both are less than those of Inconel 718 (Fig. 3c).

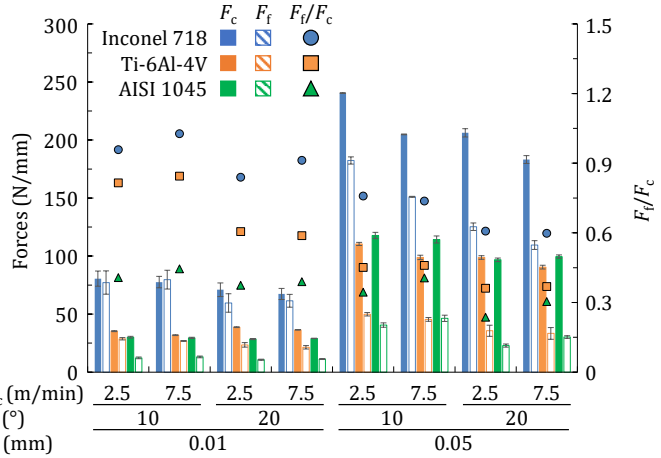

Figure 2. Cutting, feed forces, and F_f/F_c ratio for the tested conditions.

For a more detailed description, the profiles are characterised by three features, defined in the Fig. 3c inset. There is a peak of height $\Delta 1$ where the teeth enter the workpiece, a valley of depth $\Delta 2$ towards the middle of the profile, and a rise of $\Delta 3$ from the valley bottom to the exit point. The periodicity of these features match with the pitch (8 mm), as also observed by Axinte [8].

$\Delta 1$ ranges from 0.7 to 1.8 μm for AISI 1045, from 1.4 to 2.6 μm for Ti-6Al-4V, and from 4.4 to 10.8 μm for Inconel 718. For $\Delta 2$ the ranges are respectively 0.2 to 0.8 μm, 0.6 to 2.3 μm, and 1.9 to 4.7 μm; and for $\Delta 3$ they are 1.1 to 3.8 μm, 3.8 to 6.3 μm and 8.5 to 16.8 μm. When these findings are compared with the measured forces, an obvious qualitative conclusion is that feature size increases with forces. However, the ratios between feature size and forces are not equal for all three materials. Improved agreement was obtained by considering the force ratios F_f/F_c and the differences in elasticity between the materials (the Young's modulus of Inconel 718, Ti-6Al-4V, and AISI 1045 are 210 GPa, 115 GPa, and 210 GPa, respectively). This is developed in Sections 4.1 and 4.2.

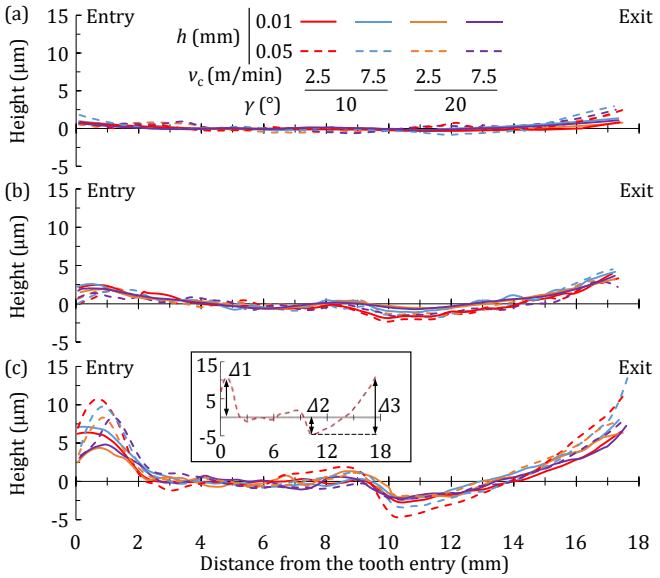

Figure 3. Surface profiles of (a) AISI 1045, (b) Ti-6Al-4V, and (c) Inconel 718. The legend in (a) applies to all three figures. (c) Includes an inset to define $\Delta 1$-$\Delta 3$; v_c = 2.5 m/min, h = 0.05 mm, and γ = 10°.

4. Discussion

4.1. Sensitivity analysis based on FEM simulations

FEM simulation was used to support interpretation of the experimental results. Its conclusions are taken forward to further discussion in Sections 4.2 and 4.3.

Results from a series of 1- and 2-tooth simulations, (using AdvantEdge2D, with the workpieces mainly at 1/3rd scale but also at half-scale), show that the surface profile after broaching was determined by mechanical effects. There were no significant thermal effects. The workpiece mechanical boundary conditions were selected after initial trials and within the constraints of the software; Fig. 4 shows a 1/3rd scale workpiece model with a 1- and 2-tooth tool (γ = 10°). On the workpiece surface, boundary conditions similar to the experimental tests (Fig. 1a) were applied. The clamping bolt action is represented along *ab* and the clamp reaction forces along *de* and *fg*. The reactions were not chosen to act along all of *ce* and *eg* as initial simulations then found tensile contact forces over the lengths approximately *cd* and *ef*. Over *ab* and *fg*, v_x = 0. Over *de*, v_y = 0. On the tool surfaces, selected as shown, $v_x = v_c$, v_y = 0. The forces F_c and F_f, moving across the surface as broaching progresses, are also shown.

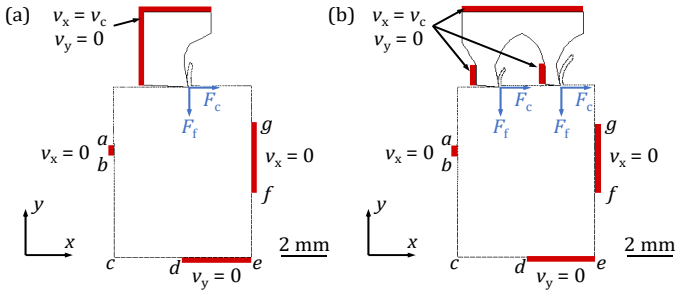

Figure 4. Mechanical boundary conditions and 1/3rd scale workpiece, for (a) single and (b) two-tooth tool simulations.

Simulations to determine $\Delta 1$-$\Delta 3$ were performed varying γ from -5 to 30° and the tool-chip sliding friction coefficient μ from 0.25 to 0.9, both to vary F_f/F_c. The Young's modulus of the workpiece E_{work} was varied from 110 to 220 GPa. E_{tool} was 220 GPa, and also 2200 GPa to eliminate tooth deflection. A work plasticity model appropriate for Inconel 718 was chosen, with simulations at a rise per tooth of 0.05 mm but carried out at v_c = 20 m/min to reduce computation time. Flow stress was varied proportionately by up to 50% to alter the force magnitudes without changing F_f/F_c.

Representative predicted profiles from 1-tooth models are shown in Fig. 5a-f. Part (a) (γ = -5°, μ = 0.9, E_{work} = E_{tool} = 220 GPa) shows a surface profile just before and after the tooth exits the workpiece. Peaks of height $\Delta 1$ and $\Delta 3$ exist at entry and exit. The profile just before exit shows compressive recovery behind the tool as the cut proceeds. After exit a further recovery occurs by an anti-clockwise rotation as shear is released. Animation of the developing profile reveals that $\Delta 1$ is due to tool spring-back. This was supported by further simulations in which E_{tool} and E_{work} were varied. Parts (b) and (c) are profiles from the same condition as (a) except that for both E_{tool} = 2200 GPa, and for (c), E_{work} = 150 GPa. In both, $\Delta 1$ is less than in (a), while reducing E_{work} does not alter $\Delta 1$. Reducing E_{work} does however, increase $\Delta 3$. Increasing γ from -5° to 10° (part d) and 30° (part e) eliminates $\Delta 1$ and reduces $\Delta 3$. It also reduces F_c and F_f/F_c. Similar changes, due to increasing γ, are caused by reducing μ (results not presented). Increasing the flow stress (part f) increases F_c without significantly changing F_f/F_c: $\Delta 3$ is increased without altering the qualitative shape of the profile. The conclusion from these examples is that the magnitude of forces and the ratio F_f/F_c are two independent variables which determine the profile. The magnitude of machining forces influences the scale of the profile while F_f/F_c influences the quality of the profile.

$\Delta 2$ is predicted in 2-tooth simulations (Fig. 5g). $\Delta 2$ is located towards the middle of the profile, as was also observed experimentally. Its position coincides with the position of the 2nd tooth when the 1st tooth exits the cut. $\Delta 2$ was found to be so sensitive to the placing of the mechanical constraints, especially *de* (Fig. 4), that its predicted values can range from positive to negative depending on the placement. Part (g) is obtained after shifting *de* towards *c*.

The predicted $\Delta 1$ and $\Delta 3$ are ≈ 0.2 times the measured values and $\Delta 2$ is also too small (when compared in the dimensionless form to be introduced in Section 4.2). A single simulation with a half-scale workpiece model in the Fig. 5a condition increases $\Delta 3$ by 1.4 times. Greater increases were produced by weakening the mechanical boundary condition constraints by reducing the lengths *de* and *fg* in Fig. 4, while keeping the positions of *e* and *g* unchanged. The underestimation of $\Delta 1$-$\Delta 3$ in the simulations was attributed to scaling and workpiece holding.

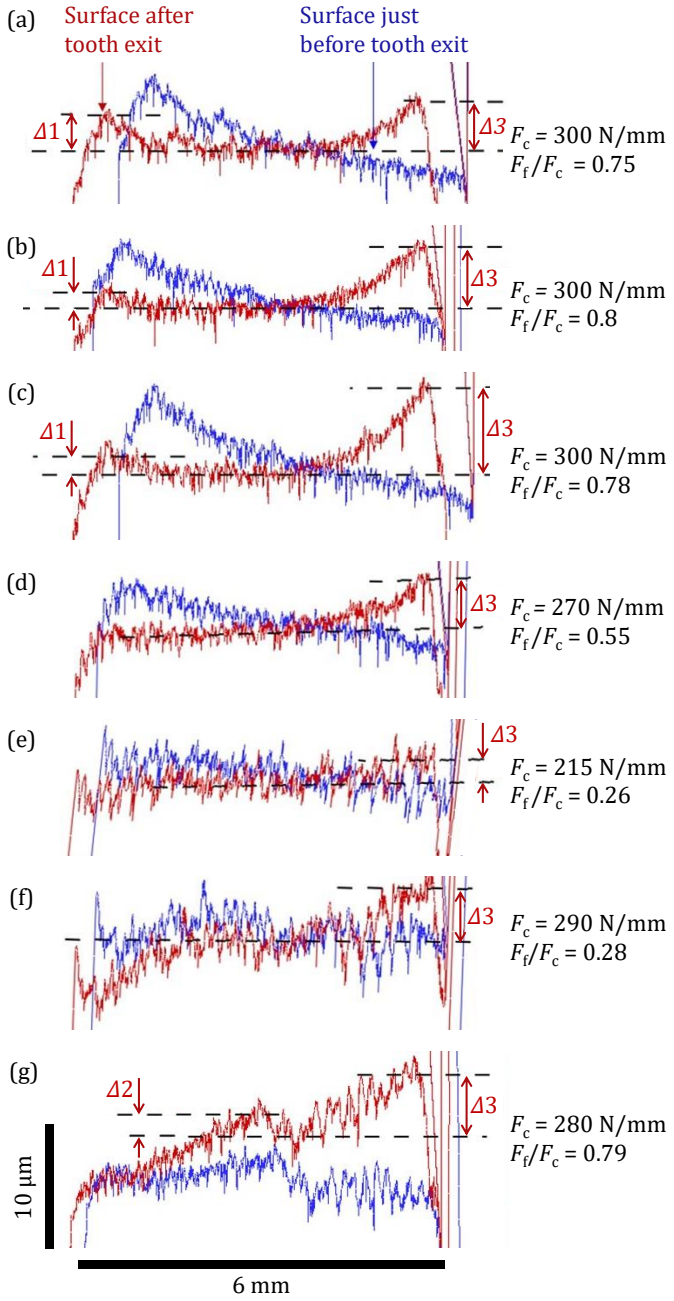

Figure 5. Surface profiles and their accompanying F_c, F_f/F_c values, (a-f) single and (g) two-tooth simulations. Input conditions: (a) γ = -5°, μ = 0.9, E_{work} = E_{tool} = 220 GPa, (b-f) as in (a) but with conditions changed as follows: (b) E_{tool} = 2200 GPa, (c) E_{tool} = 2200 GPa, and E_{work} = 150 GPa, (d) γ = 10°, (e) γ = 30°, (f) as in (e) but flow stress increased 50%, and (g) as in (a). The colour scheme and scale are the same for all parts.

4.2. Fitting of experimental results

The simulations predict that the size of the Δi, i = 1-3, depend on both F_c and F_f/F_c, and on the Young's modulus E_{work} and E_{tool}. They are used here to guide the development of quantitative equations for the experimental observations.

It is expected from elasticity mechanics that the Δi, i = 1-3, are proportional to force and inversely proportional to Young's modulus. In the present work, force is described by the components F_f and F_c. Young's modulus (E_i) may be E_{work} or E_{tool}. By linear superposition, and most generally, Δi can be expressed as in Eq. 1. This is non-dimensionalised by dividing by F_c (Eq. 2), to express Δi as proportional to the size of F_c and dependent on the force direction ratio F_f/F_c, in line with observations.

$$\Delta i\, E_i = C_{if} F_f + C_{ic} F_c \quad (1)$$

$$\Delta i\, E_i/F_c = C_{if} (F_f/F_c) + C_{ic} \quad (2)$$

The experimental Δi from Fig. 3, non-dimenionalised by F_c from Fig. 2 and by E_i, are plotted against F_f/F_c in Fig. 6. Guided by the experiments and simulations, E_i is chosen as E_{work} for $\Delta 2$ and $\Delta 3$. E_i is chosen as E_{tool} (220 GPa) for $\Delta 1$ from the simulations.

Linear regressions fit the experimental data with significantly high R^2 values. The coefficients of the regression (C_{if} and C_{ic}) and R^2 values are included in Fig. 6. Considering the results from the figure, the relationship between the Δi, E_i, F_c, and F_f/F_c are returned to the dimensional form of Eq. 1 in Eqs. 3-5.

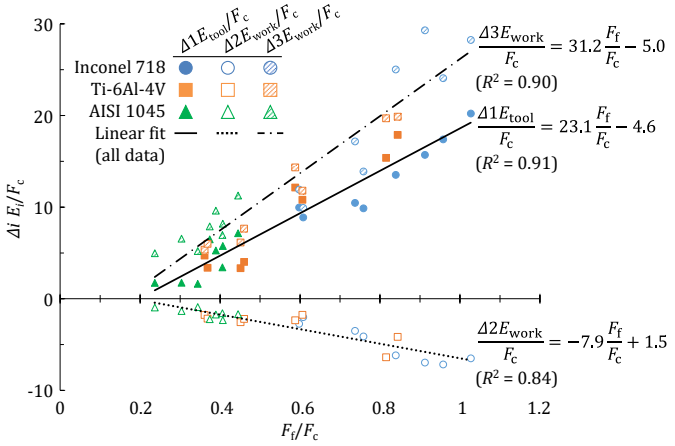

Figure 6. Linear regressions of the experimental results of $\Delta i\, E_i/F_c$ plotted against F_f/F_c.

$$\Delta 1\, E_{tool} = 23.1F_f - 4.6F_c \quad (3)$$

$$\Delta 2\, E_{work} = -7.9F_f + 1.5F_c \quad (4)$$

$$\Delta 3\, E_{work} = 31.2F_f - 5.0F_c \quad (5)$$

4.3. Practical aspects

From the experiments and simulations presented in this paper, $\Delta 3$ is largest and $\Delta 2$ is smallest and all three of $\Delta 1$–$\Delta 3$ decrease with decreasing F_c and F_f/F_c, (see Fig. 6). In practice, F_f/F_c can be reduced by increasing the tooth rake angle, limited by weakening the cutting edge. F_c can be reduced by decreasing the rise per tooth. Nevertheless, Fig. 2 illustrates that the reduction in force is less than proportional to the reduction in rise per tooth, and F_f/F_c increases when rise per tooth is reduced.

Eqs. 3-5 summarise the force influences on $\Delta 1$–$\Delta 3$. At the higher practical limit of F_f/F_c (≈ 1 from Fig. 2), all three are dominated by the F_f term. At the lower limit (F_f/F_c ≈ 0.25 from Fig. 2), the F_f and F_c terms are approximately equal for $\Delta 1$–$\Delta 3$ (Eqs. 3-5). F_f can be interpreted as causing compression and F_c as causing shear. The difference in the qualitative responses of the three workpiece materials is attributed to the relative importance of the compression and shear distortions arising from their different F_f/F_c ranges. Quantitatively, Inconel 718 has the highest forces, and Ti-6Al-4V and AISI 1045 have approximately equal forces, due to their material flow stresses. In combination, these explain the largest and clear profile variations for Inconel 718, with the least and minor profile variations for AISI 1045, with Ti-6Al-4V presenting an intermediate behaviour (Fig. 3).

There is no doubt from the simulations, supported by the experiments, that, in addition to the influences of F_c and F_f/F_c on $\Delta 2$ and $\Delta 3$, $\Delta 2$ and $\Delta 3$ increase as E_{work} reduces (the simulations predict an inverse relationship). In the case of $\Delta 1$, the simulations suggest that E_{tool} has greater influence than E_{work}. For this reason, E_{tool} is chosen for non-dimensionalisation in Fig. 6. It suggests that, whereas it is the compression and shear of the workpiece that determines $\Delta 2$ and $\Delta 3$, it is the deformation of the tool that influences $\Delta 1$. When the tool moves from the left to the right (Fig. 1a), F_f deflects the tool in the anti-clockwise direction, raising the tooth and therefore increasing $\Delta 1$. In contrast, F_c deforms the tooth in the clockwise direction, balancing and moving the tooth down from the higher deformation caused by F_f. It suggests that the design of the geometry of the tooth is key to preventing high deformations at the moment the tool enters the workpiece. A different consideration applies to $\Delta 2$. Increasing the last tooth pitch to greater than the work length would remove it.

Thus, this work achieves its objective of understanding the phenomena involved in the topography irregularities that arise in broaching. In particular, it sheds light on the role of materials response to chip formation that determines broaching forces under different cutting conditions. This is in addition to system dynamic effects that are the subject of previous works [8].

5. Summary and conclusions

The influence of cutting conditions and tool geometry on surface profiles obtained from broaching Inconel 718, Ti-6Al-4V and AISI 1045 was studied experimentally in conditions close to industry. High peaks were observed at tooth entry and exit positions, with valleys towards the mid-point. Major differences in scale and relative differences between the features occurred between the three materials. Cutting and feed forces were also measured, with the largest forces obtained for Inconel 718 and similar levels of lower forces for Ti-6Al-4V and AISI 1045. The feed to cutting force ratio also differed between the materials.

Simulations support the experiments. They predict how the cut surface profile depends on the Young's modulus of the tool and workpiece, as well as the broaching force magnitude and direction. The differences between these explains the differences between the profiles observed experimentally. The simulations guide linear regression fitting between the experimental profile features and forces. New insight is gained into how the broached profiles depend on chip formation, separately from dynamic systems effects that also are known to be important.

Acknowledgements

The authors thank the INTOOL II (KK-2020/00103) and SURFNANOCUT (RTI2018_095463-B-C21/C22) projects, as well as the grant for Education and Training of Research Staff (PRE_2017_1_0394).

References

[1] Arrazola, P. J., Rech, J., M'Saoubi, R., Axinte, D., 2020, Broaching: Cutting tools and machine tools for manufacturing high quality features in components, Annals of the CIRP, 69/2: 554–577.

[2] European Commission, 2019, Innovative Method dedicated to the development of a ferrite-pearlite grade regarding its Machinability (IMMAC): final report.

[3] M'Saoubi, R., Axinte, D., Soo, S. L., Nobel, C., Attia, H., Kappmeyer, G., Engin, S., Sim, W. M., 2015, High performance cutting of advanced aerospace alloys and composite materials, Annals of the CIRP, 64/2: 557–580.

[4] Arrazola, P. J., Garay, A., Armendia, M., Marya, S., Le Maitre, F., 2009, Machinability of titanium alloys (Ti6Al4V and Ti555.3), J. Mater. Process. Technol., 209/5: 2223–2230.

[5] Axinte, D., Boud, F., Penny, J., Gindy, N., Williams, D. J., 2005, Broaching of Ti-6-4-Detection of workpiece surface anomalies on dovetail slots through process monitoring, Annals of the CIRP, 54/1: 87–90.

[6] Davim, J. P., 2010, Surface integrity in machining, Springer.

[7] Cubberly, W. H., 1989, Tool and Manufacturing Engineers Handbook Desk Edition, Society of manufacturing engineers.

[8] Axinte, D. A., 2007, An experimental analysis of damped coupled vibrations in broaching, Int. J. Mach. Tools Manuf., 47/14: 2182–2188.

[9] Arrieta, H. V., Wackers, P., Van, K. D., Constantinescu, A., Maitournam, H., 2003, Modelling Attempts to Predict Fretting-Fatigue Life on Turbine Components, RTO-MP-AVT-109.

Declaration of interests

☒ The authors declare that they have no known competing financial interests or personal relationships that could have appeared to influence the work reported in this paper.

☐The authors declare the following financial interests/personal relationships which may be considered as potential competing interests:
